On the use of short-time Fourier transform and synchrosqueezing-based demodulation for the retrieval of the modes of multicomponent signals

Sylvain Meignen, Duong-Hung Pham, Marcelo Colominas

Version of Record: https://www.sciencedirect.com/science/article/pii/S0165168420303030
Manuscript_758b380203616eae2986e105e2ac2a3a

On the Use of Short-Time Fourier Transform and Synchrosqueezing-Based Demodulation for the Retrieval of the Modes of Multicomponent Signals

Sylvain Meignen[1], Duong-Hung Pham[2] and Marcelo A. Colominas[3] [1]
[1]Jean Kuntzmann Laboratory- Bâtiment IMAG,
Université Grenoble Alpes
700 Avenue Centrale
Campus de Saint Martin d'Hères
38401 Domaine Universitaire de Saint-Martin-d'Hères, France
[2]IRIT Laboratory
Paul Sabatier University
118 route de Narbonne
31400 Toulouse, France
[3] Institute for Research and Development in Bioengineering and Bioinformatics (IBB)
CONICET, Ruta Prov. 11 Km. 10, Oro Verde
Entre Ríos, Argentina

Abstract

In this paper, our goal is to compare different recent *time-frequency* (TF) approaches to retrieve the modes of *multicomponent signals* (MCSs). While it is acknowledged that the *synchrosqueezing transform* (SST) improves the readability of the *time-frequency representation* (TFR) of the modes of MCSs, and that *SST-based demodulation* (DSST) is more efficient than SST itself for *mode retrieval* (MR), it is unclear whether DSST outperforms downsampled *short-time Fourier transform* (STFT) in that matter. The goal of the present paper is to answer this question and to propose a variant of DSST that reduces mode-mixing. The focus is put on the sensitivity of the different techniques to frequency modulation for the modes and frequency resolution.

Keywords: Time-frequency analysis, downsampled short-time Fourier transform, AM/FM multicomponent signals, mode retrieval, synchrosqueezing, synchrosqueezing-based demodulation.

[1]This work was partly supported by "Agence National pour la recherche" under grant ANR-19-CE48-0001-01.

1. Introduction

The last few years have witnessed an upsurge of interest from the signal processing community over MCSs, defined as the superimposition of amplitude and frequency modes. Indeed, these possess the ability to accurately represent *non-stationary* signals commonly encountered in practical non-linear systems as, for instance in pathology diagnosis [1, 2], structural stability [3, 4] or physiology [5]. To analyze such signals, linear TFRs such as the *continuous wavelet transform* or STFT have attracted overwhelming attention. The effectiveness of these transforms is however constrained by the choice of an analysis window which can never be ideal due to Heisenberg uncertainty principle. To circumvent this issue, *reassignment methods* were introduced in [6] and further developed in [7], undeniably improving the readability of the TFRs they are based on. But since MR is no longer possible from the reassigned transforms, to cope with this issue a variant called *synchrosqueezing transform* (SST) was introduced. Initially developed in the wavelet context [8] and then extended to STFT [9], SST allows for accurate reconstruction of slightly modulated modes. To deal with MCSs containing modes with non-negligible frequency modulation, an extension of SST based on a linear chirp approximation was proposed in [10, 11] and then a generalization to modes with fast oscillating phase was introduced in [12]. Besides, SST can be used to build a demodulation algorithm, called DSST, that outperforms SST for MR. It was first introduced in [13] and further improved in [14, 15]. Alternative approaches were also developed formulating MR either as a convex optimization problem [16], or by performing it the *empirical mode decomposition* [17], the *empirical wavelet transform* [18], or *variational mode decompositions* [19]. These techniques share the property that they extract band-limited modes, and are in that matter different from the above mentioned TF techniques.

While SSTs are very efficient to localize the information in the TF plane, the benefit of using DSST rather than STFT for MR is still unclear. Indeed, as explained in [20], the same quality of MR can be attained with time-downsampled STFT as with DSST using much less TF coefficients. Nevertheless, the conclusions in [20] do not reflect the recent advances in the designing of DSST [14, 15]. Our goal in this paper is therefore to clearly state in which circumstances DSST offers better MR performance than downsampled STFT, of which we propose a variant limiting mode mixing. In particular, we will focus on the behavior of the above mentioned techniques when the frequency modulation of the modes and the frequency resolution vary.

The layout of the paper is as follows: in Section 2, we recall basic definitions and notations that we use throughout the paper. Then we briefly recall, in Section 3, how to perform MR using DSST and downsampled STFT. Finally, we conclude the paper by comparing the different approaches in Section 4, clearly stating whether reassigning STFT is interesting for MR.

2. Definitions and Notations

2.1. Short-Time Fourier Transform

The STFT of $f \in L^1(\mathbb{R})$ is defined by (g being a real window in $L^\infty(\mathbb{R})$):

$$V_f^g(t,\xi) = \int_{\mathbb{R}} f(\tau) g(\tau - t) e^{-2i\pi\xi(\tau - t)} d\tau = \int_{\mathbb{R}} f(t+\tau) g(\tau) e^{-2i\pi\xi\tau} d\tau. \quad (1)$$

When f is with finite length L corresponding to samples $f(\frac{nT}{L})_{n=0,\cdots,L-1}$, and g supported on $[-\frac{MT}{L}, \frac{MT}{L}]$ with $M < L/2$, one has:

$$V_f^g(\frac{mT}{L}, \frac{kL}{N_0 T}) \approx \mathbf{V}_f^g[m,k] := \frac{T}{L} \sum_{n=-M}^{M} f\left(\frac{(m+n)T}{L}\right) g\left(\frac{nT}{L}\right) e^{-i2\pi\frac{nk}{N_0}}, \quad (2)$$

for some $N_0 \geq 2M+1$. Denoting $f[n] = f\left(\frac{nT}{L}\right)$ and $g[n] = g\left(\frac{nT}{L}\right)$, one obtains:

$$\mathbf{V}_f^g[m,k] = \frac{T}{L} \sum_{n=0}^{2M} f[m+n-M] g[n-M] e^{-i2\pi\frac{k(n-M)}{N_0}}, \quad (3)$$

the downsampled STFT by a factor of R corresponding to $\mathbf{V}_f^g[mR,k]$.

2.2. Definition of MCS

In this paper, we study MCSs defined as a superimposition of modes:

$$f(t) = \sum_{p=1}^{P} f_p(t), \quad \text{with} \quad f_p(t) = A_p(t) e^{i2\pi\phi_p(t)}, \quad (4)$$

where $A_p(t)$ and $\phi_p'(t)$ are respectively the instantaneous amplitude (IA) and frequency (IF) of f_p satisfying $A_p(t) > 0, \phi_p'(t) > 0$ and $\phi_{p+1}'(t) > \phi_p'(t)$ for all t.A_p is assumed to be differentiable with $|A_p'(t)|$ small compared to $\phi_p'(t)$, and the modes are separated with resolution Δ:

$$\forall t,\ \forall 1 \leq p \leq P-1,\ \phi_{p+1}'(t) - \phi_p'(t) > 2\Delta. \quad (5)$$

2.3. Window Determination Based on Rényi Entropy

To compute the STFT of MCSs, a crucial aspect is the determination of an appropriate window, which is often done by considering the minimal Rényi entropy [21, 22, 13, 20]. For the sake of simplicity, we stick to this approach though we are aware of recent developments on the computation of STFT and wavelet transforms based on adaptive window determination [23][24].

3. An overview of MR Techniques Based on STFT

3.1. STFT-Based Synchrosqueezing Transforms

The *STFT-based synchrosqueezing transform* (SST) is based on the definition of the *local instantaneous frequency (IF)* $\widehat{\omega}_f$, wherever $V_f^g(t,\xi) \neq 0$ [7]:

$$\widehat{\omega}_f(t,\xi) = \frac{\partial \arg V_f^g(t,\xi)}{\partial t} = \Re\left\{\frac{1}{2i\pi}\frac{\partial_t V_f^g(t,\xi)}{V_f^g(t,\xi)}\right\}, \tag{6}$$

and consists of moving any coefficient $V_f^g(t,\xi)$ with magnitude larger than γ to location $(t,\widehat{\omega}_f(t,\xi))$:

$$T_f^\gamma(t,\omega) = \int_{|V_f^g(t,\xi)|>\gamma} V_f^g(t,\xi)\delta(\omega - \widehat{\omega}_f(t,\xi))d\xi. \tag{7}$$

One can define a discrete-time version of $\widehat{\omega}_f(t,\xi)$ and then of $T_f^\gamma(t,\omega)$, that we denote by $\mathbf{T}_f^\gamma$. The applicability of SST being restricted to MCSs made of slightly perturbed purely harmonic modes, an extension based on linear chirp approximation and called *second-order STFT-based synchrosqueezing transform* (SST2) [10, 11] was introduced. It uses a more accurate IF estimate than $\widehat{\omega}_f$ denoted by $\widehat{\omega}_f^{[2]}(t,\xi)$, the construction of which is detailed in [11], and SST2 is defined replacing $\widehat{\omega}_f(t,\xi)$ by $\widehat{\omega}_f^{[2]}(t,\xi)$ in (7), to obtain $T_{2,f}^\gamma$ and its discrete-time counterpart $\mathbf{T}_{2,f}^\gamma$. To handle signals containing more general types of modes with non-negligible $\phi^{(k)}(t)$ for $k \geq 3$, new modulation operators based on higher approximations of both amplitude and phase were defined [12], resulting in new IF estimates $\widehat{\omega}_f^{[N]}(t,\xi)$ and the N^{th}-order SST (SSTN) is defined by replacing $\widehat{\omega}_f(t,\xi)$ by $\widehat{\omega}_f^{[N]}(t,\xi)$ in (7) to obtain $T_{N,f}^\gamma(t,\omega)$ and its discrete-time counterpart $\mathbf{T}_{N,f}^\gamma$.

3.2. Ridge Detection

A pivotal step in MR techniques based on TFR is ridge detection (RD), for which, in this paper, we adopt the same approach as in [8, 7], and originally proposed in [25]. The goal is to compute an estimate $\varphi_p(t)$ of $\phi_p'(t)$ by extracting on the TFR a ridge associated with mode p. This is carried out using a *peeling algorithm* at the end of which a set of ridges $(\varphi_p)_{p=1,\cdots,P}$ is extracted (for details see for instance [26]).

3.3. Demodulation Algorithm Based on SSTN for Mode Reconstruction

We here recall the concept of demodulation based on SSTN, denoted by DSSTN, first introduced in the SST2 context [13], further improved in [14] and extended to SSTN in [15]. The basic idea is to replace the IF estimate φ_p given by RD (recalled in Section 3.2) by either $\widehat{\omega}_f(t,\varphi_p(t))$, $\widehat{\omega}_f^{[2]}(t,\varphi_p(t))$, or $\widehat{\omega}_f^{[N]}(t,\varphi_p(t))$, when either SST, SST2, or SSTN are used. One then considers Algorithm 1, proposed in [13] to recover the modes.

Algorithm 1 Demodulation based on SSTN (DSSTN)

Input: Constant frequency ψ_0, $(\tilde{\varphi}_p(t) = \widehat{\omega}_f^{[N]}(t, \varphi_p(t)))_{p=1,\cdots,P}$.
for $p = 1$ to P **do**

1. Compute $f_{D,p}(t) = f(t)e^{-i2\pi(\int_0^t \tilde{\varphi}_p(x)dx - \psi_0 t)}$.
2. From $T^{\gamma}_{f_{D,p}}$, extract $\varphi_{D,p} \in [\psi_0 - \Delta, \psi_0 + \Delta]$ (ridge of p^{th} mode of $f_{D,p}$).
3. Retrieve p^{th} mode of $f_{D,p}$ and inverse demodulation to retrieve f_p:

$$f_p(t) \approx \left(\int_{|\omega - \varphi_{D,p}(t)| < d_{IF}} T^{\gamma}_{f_{D,p}}(t,\omega)d\omega\right) e^{i2\pi(\int_0^t \tilde{\varphi}_p(x)dx - \psi_0 t)},$$

where d_{IF} is a parameter compensating for errors due to IF estimation.

3.4. Mode Reconstruction From Downsampled STFT

Mode f_p in [20] is retrieved using two functions η_p^- and η_p^+ such that the information relative to f_p at time indexed by mR is mostly contained in interval $J_p[mR] = [\eta_p^-[mR], \eta_p^+[mR]]$. The reconstruction formula then follows:

$$f_p[n] \approx \frac{L}{T} \frac{\sum_{m\in\mathbb{Z}} \sum_{k\in J_p[mR]} \mathbf{V}_f^g[mR \mod L, k] g[n-mR] \frac{e^{i2\pi \frac{k(n-mR)}{N_0}}}{N_0}}{\sum_{m\in\mathbb{Z}} g[n-mR]^2}, \tag{8}$$

where mod stands for modulo, provided $\sum_{m\in\mathbb{Z}} g[n-mR]^2 \neq 0$ for all n. To define η_p^- and η_p^+, a first strategy [20] is to consider a noisy version of f, $\tilde{f}[n] = f[n] + \sigma\Phi[n]$, with $\Phi[n]$ a unit variance, zero mean, Gaussian noise and then put:

$$\begin{aligned} \eta_p^-[mR] &:= \operatorname*{argmax}_k \left\{ k < \varphi_p[mR], |\mathbf{V}_{\tilde{f}}^g[mR,k]| < 3\sigma\|g\|_2 \right\} \\ \eta_p^+[mR] &:= \operatorname*{argmin}_k \left\{ k > \varphi_p[mR], |\mathbf{V}_{\tilde{f}}^g[mR,k]| < 3\sigma\|g\|_2 \right\}, \end{aligned} \tag{9}$$

the threshold $3\sigma\|g\|_2$ being set remarking that $\frac{|\mathbf{V}_{\sigma\Phi}^g[mR,k]|^2}{\sigma^2\|g\|_2^2}$ is χ^2 distributed with 2 degrees of freedom [20] (probability of false alarm lesser than 1%). As this approach results in a too large interval $J_p[mR]$ when the noise level is low and when f_p and f_{p+1} slightly interfere in the TF plane at some time index mR (meaning the separation condition (5) is not exactly satisfied), mode-mixing occurs in such situations ($|\mathbf{V}_{\tilde{f}}^g[mR,k]|$ remains larger than $3\sigma\|g\|_2$ when k varies in $[\varphi_p[mR], \varphi_{p+1}[mR]]$). To overcome this limitation, we slightly modify (9), replacing $J_p[mR]$ by $J_{1,p}[mR] := [\eta_{1,p}^-[mR], \eta_{1,p}^+[mR]]$ with:

$$\begin{aligned} \eta_{1,p}^-[mR] &:= \max\left\{ \eta_p^-[mR], \varphi_p[mR] - \lfloor \frac{\Delta N_0 T}{L} \rceil \right\} \\ \eta_{1,p}^+[mR] &:= \min\left\{ \eta_p^+[mR], \varphi_p[mR] + \lfloor \frac{\Delta N_0 T}{L} \rceil \right\}, \end{aligned} \tag{10}$$

where $\lfloor X \rceil$ denotes the nearest integer to real X. By modifying definition (9) into (10), one imposes that $[\eta^-_{1,p}[mR], \eta^+_{1,p}[mR]] \subset [\varphi_p[mR] - \lfloor \frac{\Delta N_0 T}{L} \rceil, \varphi_p[mR] + \lfloor \frac{\Delta N_0 T}{L} \rceil]$, so that mode-mixing due to errors in the computation of J_p should be overcome. In what follows, when performing MR comparisons in Section 4, the method based on (9) (resp. (10)) is denoted by $STFT\text{-}M_1$ (resp. $STFT\text{-}M_2$).

4. Comparison of MR Techniques

In this section, our goal is to compare the quality of MR obtained by using either DSSTN or downsampled STFT. We first investigate the influence of frequency modulation of the modes on MR, in Section 4.1, and then of the frequency resolution as well as the number of TF coefficients used for MR in each case, in Section 4.2 . To study all these aspects, we consider three different types of signals whose STFT moduli are displayed in Fig. 1. The first one is a signal made of a linear and a quadratic chirp (Fig. 1 (a)), the second is composed of two modes with cosine phase (Fig. 1 (b)), while the third one is a mode with a highly oscillatory cosine phase. The MR performance are evaluated through $\mathrm{SNR}_{\mathrm{output}} = 20 \log_{10} \left(\|f_p\|_2 / \|f_{p,r} - f_p\|_2 \right)$, where $f_{p,r}$ is the reconstructed p^{th} mode and $\|.\|_2$ is the l_2 norm. Though somehow arbitrary, the choice for test signals we make is related to the different aspects we would like to put forward, in particular how the studied methods cope with close modes, when the frequency modulation is low, typically as in the signal of Fig. 1 (a), or higher as in Fig. 1 (b). The example of Fig. 1 (c) finally enables to test how the methods deal with frequency modulation only, mode separation being not an issue in that case.

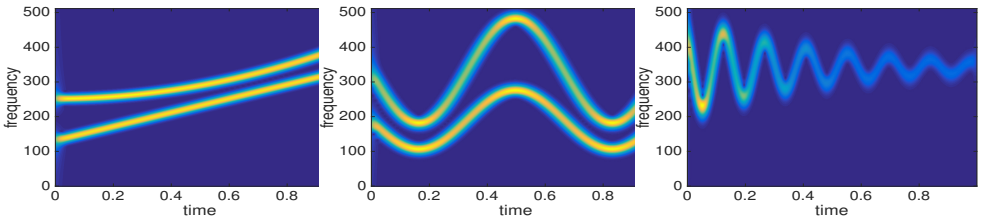

Figure 1: STFT modulus of (a): a linear and a quadratic chirp; (b): two modes with cosine phase; (c): a signal with a highly oscillating cosine phase.

4.1. Robustess to Frequency Modulation of MR Techniques

First of all, we explore the robustness to frequency modulation of MR either based on DSSTN (for $N = 2$, 3 or 4), $STFT\text{-}M_1$ or $STFT\text{-}M_2$ (for these last two techniques the downsampling parameter R is specified in each simulation).

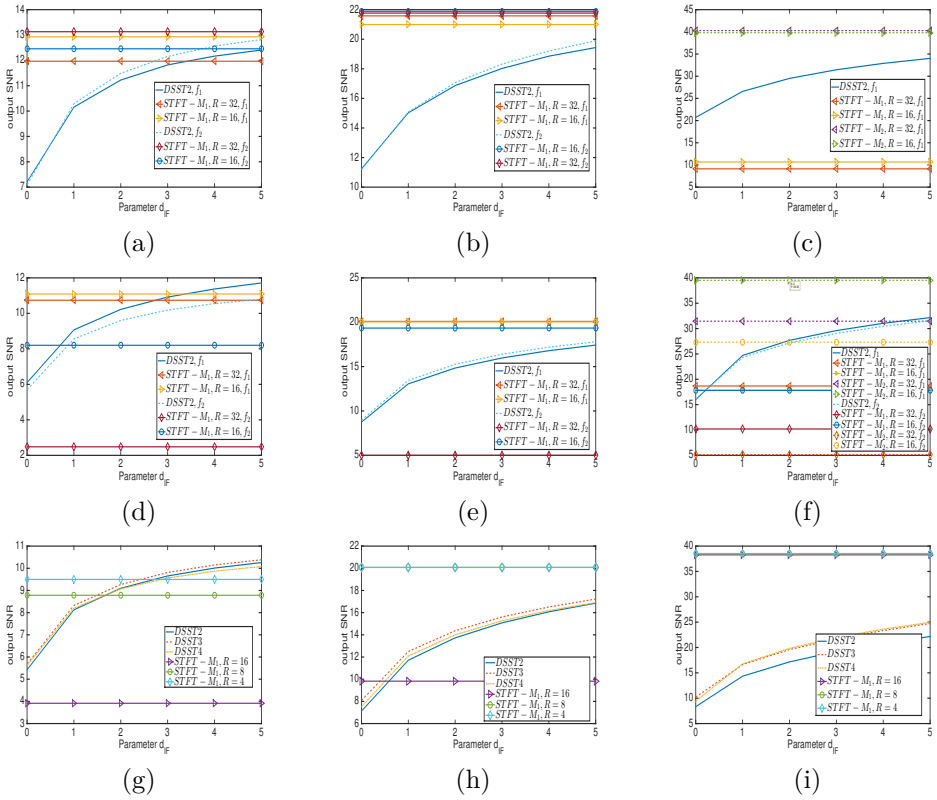

Figure 2: (a): MR results for the signal displayed in Fig. 1 (a) when $N_0 = L$, using either *DSST2*, *STFT*-M_1 when the input SNR is 0 dB; (b): Same as (a) except the input SNR is 10 dB; (c): Same as (a) except the input SNR is 30 dB and the results obtained with *STFT*-M_2 are also displayed (and only mode f_1 is considered); (d): Same as (a) but for the signal of Fig. 1 (b); (e): Same as (d) except the input SNR is 10 dB; (f): Same as (d) except the input SNR is 30 dB and the results obtained with *STFT*-M_2 are also displayed; (g): Same as (a) but for the signal of Fig. 1 (c) (*DSST3* and *DSST4* are also tested); (h): Same as (g) except the input SNR is 10 dB; (e): Same as (g) except the input SNR is 30 dB.

In Fig. 2, we depict MR results, when the noise level varies and when $N_0 = L$ in STFT computations, corresponding to the output SNR with respect to the parameter d_{IF} mentioned in Algorithm 1. As neither *STFT*-M_1 nor *STFT*-M_2 depend on d_{IF}, with such methods the output SNR is constant. The first row of Fig. 2 corresponds to MR results for the signal of Fig. 1 (a). For that signal, since *DSST3* and *DSST4* behave similarly to *DSST2*, only the results related to the latter are reported. We first remark that *STFT*-M_1 is only slightly sensitive to the downsampling factor R, when the input SNR equals 0 or 10 dB (similar results are obtained with *STFT*-M_2). Very close results are obtained with *DSST2* by choosing a large enough d_{IF}. At low noise level (30 dB, see Fig. 2 (c)), the interval $J_p[mR]$ used in *STFT*-M_1 is too large for

some time instants, causing mode-mixing and resulting in inaccurate MR. On the contrary, the variant we propose, *STFT-*M_2, behaves nicely, is insensitive to R and also leads to better results than *DSST2*. For *STFT-*M_1 and *STFT-*M_2, since the MR results for the two modes are similar, we only report those related to f_1. When stronger frequency modulations are considered as in the signal of in Fig. 1 (b), the corresponding MR results on the second row of Fig. 2 are also very instructive. At 0 and 10 dB, MR performance using *STFT-*M_1 or *STFT-*M_2 are still very similar, so we only display the results with the former technique. This time, *STFT-*M_1 is very sensitive to the choice of R for mode f_2, containing the strongest frequency modulation, and, in such a case, R should be chosen relatively small to preserve the quality of MR. As for the first signal, one remarks that *DSST2* leads to similar results as those obtained with *STFT-*M_1 computed with an appropriate R. When the input SNR equals 30 dB, comparing the results corresponding to *STFT-*M_1 and *STFT-*M_2, the latter appears to deal much better with mode-mixing, provided R is still chosen sufficiently small. But even in that case, MR results for f_1 are better than those for f_2 when using *STFT-*M_2 while the quality of reconstruction with *DSST2* is the same for the two modes, meaning the latter technique is less sensitive to frequency modulation. Let us finally take a look at MR results for the mode displayed in Fig. 1 (c). Since there is only one mode to consider *STFT-*M_2 is useless here. We notice that *STFT-*M_1 leads to satisfactory results whatever the noise level when R is small enough, the sensitivity to R diminishing with the noise level. When using *DSST3* or *DSST4* instead of *DSST2*, MR results are improved but only at low noise level suggesting a sensitivity of higher order reassignment operators to noise level.

4.2. Sensitivity to Frequency Resolution of MR Techniques

To study the sensitivity of MR techniques to frequency resolution, we set N_0 to $L/4$ and redo the above computations to generate Fig. 3. By using a coarser frequency resolution, a sparser TFR of signals can be achieved, and MR can be performed with fewer TF coefficients for all the tested methods. When using DSSTN, it means that better MR results are achieved for a given d_{IF}. More precisely, since we have divided the frequency resolution by a factor of 4, to get results similar to those of Fig. 2, d_{IF} should be four times smaller than in that case (this can be actually checked by comparing the results related to *DSST2* for $d_{IF} = 4$ or $d_{IF} = 1$ for Fig. 2 and 3 respectively). It is also worth noting that *DSST2* is sensitive to d_{IF} when the noise level varies: this could have been checked at larger frequency resolution considering larger values for d_{IF}. Now regarding *STFT-*M_1 and *STFT-*M_2, comparing the results on the first rows of Fig. 2 and Fig. 3, we notice that their behaviors are very similar when the frequency resolution varies, but MR is carried out with fewer coefficients when the frequency resolution decreases. In all the three test cases, as the decrease in frequency resolution leads to a sparser TFR, fewer coefficients are needed for MR, inducing better performance of *DSST2* with respect to parameter d_{IF} (and also of *DSSTN* for highly frequency modulated modes). On the contrary,

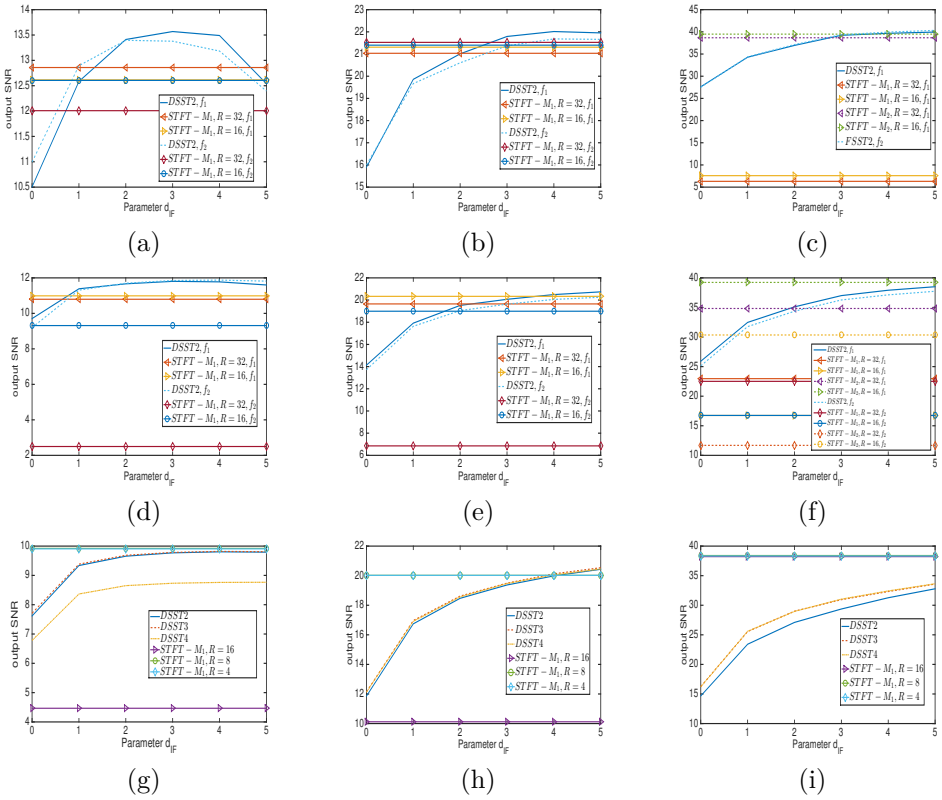

Figure 3: (a): MR results for the signal of Fig. 1 (a) when $N_0 = L/4$, using either *DSST2* or *STFT-*M_1 when the input SNR is 0 dB; (b): Same as (a) except the input SNR is 10 dB; (c): Same as (a) except the input SNR is 30 dB and we consider only mode f_1 (we also display the results for *STFT-*M_2); (d): Same as (a) but for the signal of Fig. 1 (b) when the input SNR is 0 dB; (e): Same as (d) except the input SNR is 10 dB; (f): Same as (d) except the input SNR is 30 dB (we also display the results for *STFT-*M_2);; (g): Same as (a) but for the signal of Fig. 1 (c) using either *DSST2*, *DSST3*, *DSST4*, or *STFT-*M_1, when the input SNR is 0 dB; (h): Same as (g) except the input SNR is 10 dB; (e): Same as (g) except the input SNR is 30 dB.

the quality of MR associated with *STFT-*M_1 or *STFT-*M_2 is very similar to the case $N_0 = L$, but fewer coefficients are involved in the reconstruction process. To quantify this, we compute the number of coefficients used in MR in the cases leading to the best results in the previous simulations. We remark that the number of coefficients used by *DSST2* at each time instant is $N_{demod}(d_{IF}) = P(2d_{IF}+1)$, while those used at time indexed by mR is $\sum_{p=1}^{P} \#J_p[mR]$ (in which $\#X$ is the cardinal of X) for *STFT-*M_1 or *STFT-*M_2. So the total number of coefficients used divided by L reads: $N_{STFT}(R) = \sum_m \sum_{p=1}^{P} \#J_p[mR]/L$. We thus compare N_{demod} and N_{STFT}, when $N_0 = L/4$, R and d_{IF} being set to obtain similar MR quality with *DSST2* and *STFT-*M_2. The results depicted in Table 1 tell us that in any case, to obtain MR results of similar quality with

Fig. 1 (a)	SNR = 0 dB	$(N_{STFT}(16), N_{demod}(3)) = (0.91, 14)$
	SNR = 10 dB	$(N_{STFT}(16), N_{demod}(4)) = (1.3, 18)$
	SNR = 30 dB	$(N_{STFT}(16), N_{demod}(5)) = (1.8, 22)$
Fig. 1 (b)	SNR = 0 dB	$(N_{STFT}(16), N_{demod}(3)) = (1.19, 14)$
	SNR = 10 dB	$(N_{STFT}(16), N_{demod}(5)) = (1.8, 22)$
	SNR = 30 dB	$(N_{STFT}(16), N_{demod}(5)) = (2.10, 22)$
Fig. 1 (c)	SNR = 0 dB	$(N_{STFT}(8), N_{demod}(5)) = (1, 11)$
	SNR = 10 dB	$(N_{STFT}(8), N_{demod}(5)) = (1.93, 11)$
	SNR = 30 dB	$(N_{STFT}(8), N_{demod}(5)) = (2.12, 11)$

Table 1: First row: proportion of coefficients used in $STFT\text{-}M_2$ for MR given by $N_{STFT}(R)$ and those involved in $DSST2$, given by $N_{demod}(d)$, for the signal of Fig. 1 (a); second row: same as in the first row except the studied signal is the one given in Fig. 1 (b); third row: same as in the first row except the studied signal is the one given in Fig. 1 (c) and $STFT\text{-}M_1$ is used instead of $STFT\text{-}M_2$. $N_0 = L/4$ in all cases.

DSST2 and with $STFT\text{-}M_2$, the former involves much more TF coefficients than the latter.

5. Conclusion

In this paper, our goal was to compare the reconstruction of the modes of multicomponent signals using techniques based either on downsampled STFT or on synchrosqueezing-based demodulation, of which we have introduced a variant avoiding mode-mixing. We have showed that with the former type of technique good reconstruction results imply a relatively small downsampling factor when dealing with frequency modulated signals and that a low frequency resolution improved the quality of reconstruction for the latter type of technique. We have finally reached the conclusion that, in most cases, downsampled STFT behaves similarly to synchrosqueezing-based demodulation for mode reconstruction, provided the parameters of the two techniques are correctly tuned, but the former type of techniques uses much fewer TF coefficients for mode reconstruction, therefore reassigning the STFT does not seem beneficial for that purpose.

[1] U. R. Acharya, K. P. Joseph, N. Kannathal, L. C. Min, and J. S. Suri, "Heart rate variability," in *Advances in cardiac signal processing*. Springer, 2007, pp. 121–165.

[2] M. Malik and A. J. Camm, *Dynamic electrocardiography*. John Wiley & Sons, 2008.

[3] M. Costa, A. A. Priplata, L. A. Lipsitz, Z. Wu, N. E. Huang, A. L. Goldberger, and C.-K. Peng, "Noise and poise: Enhancement of postural complexity in the elderly with a stochastic-resonance-based therapy," *Europhysics Letters (EPL)*, vol. 77, no. 6, p. 68008, Mar 2007.

[4] D. A. Cummings, R. A. Irizarry, N. E. Huang, T. P. Endy, A. Nisalak, K. Ungchusak, and D. S. Burke, "Travelling waves in the occurrence of dengue haemorrhagic fever in Thailand," *Nature*, vol. 427, no. 6972, pp. 344 –347, Jan 2004.

[5] C. L. Herry, M. Frasch, A. J. Seely, and H.-T. Wu, "Heart beat classification from single-lead ecg using the synchrosqueezing transform," *Physiological Measurement*, vol. 38, no. 2, pp. 171–187, 2017.

[6] K. Kodera, C. D. Villedary, and R. Gendrin, "A new method for the numerical analysis of non-stationary signals," *Physics of the Earth and Planetary Interiors*, vol. 12, no. 23, pp. 142 – 150, 1976.

[7] F. Auger and P. Flandrin, "Improving the readability of time-frequency and time-scale representations by the reassignment method," *IEEE Transactions on Signal Processing*, vol. 43, no. 5, pp. 1068–1089, 1995.

[8] I. Daubechies, J. Lu, and H.-T. Wu, "Synchrosqueezed wavelet transforms: an empirical mode decomposition-like tool," *Applied and Computational Harmonic Analysis*, vol. 30, no. 2, pp. 243–261, 2011.

[9] T. Oberlin, S. Meignen, and V. Perrier, "The Fourier-based synchrosqueezing transform," in *2014 IEEE International Conference on Acoustics, Speech and Signal Processing (ICASSP)*, May 2014, pp. 315–319.

[10] ——, "Second-order synchrosqueezing transform or invertible reassignment? Towards ideal time-frequency representations," *IEEE Transactions on Signal Processing*, vol. 63, no. 5, pp. 1335–1344, March 2015.

[11] R. Behera, S. Meignen, and T. Oberlin, "Theoretical analysis of the second-order synchrosqueezing transform," *Applied and Computational Harmonic Analysis*, vol. 45, no. 2, pp. 379–404, 2018.

[12] D. H. Pham and S. Meignen, "High-order synchrosqueezing transform for multicomponent signals analysis-with an application to gravitational-wave signal." *IEEE Trans. Signal Processing*, vol. 65, no. 12, pp. 3168–3178, 2017.

[13] S. Meignen, D.-H. Pham, and S. McLaughlin, "On demodulation, ridge detection, and synchrosqueezing for multicomponent signals," *IEEE Transactions on Signal Processing*, vol. 65, no. 8, pp. 2093–2103, 2017.

[14] S. Meignen, T. Oberlin, and D.-H. Pham, "Synchrosqueezing transforms: From low-to high-frequency modulations and perspectives," *Comptes Rendus Physique*, vol. 20, no. 5, pp. 449–460, 2019.

[15] D.-H. Pham and S. Meignen, "Demodulation algorithm based on higher order synchrosqueezing," in *2019 27th European Signal Processing Conference (EUSIPCO)*. IEEE, 2019, pp. 1–5.

[16] M. Kowalski, A. Meynard, and H.-T. Wu, "Convex optimization approach to signals with fast varying instantaneous frequency," *Applied and Computational Harmonic Analysis*, vol. 44, no. 1, pp. 89–122, Jan 2018. [Online]. Available: https://doi.org/10.1016/j.acha.2016.03.008

[17] N. E. Huang, Z. Shen, S. R. Long, M. C. Wu, H. H. Shih, Q. Zheng, N.-C. Yen, C. C. Tung, and H. H. Liu, "The empirical mode decomposition and the hilbert spectrum for nonlinear and non-stationary time series analysis," *Proceedings of the Royal Society of London. Series A: Mathematical, Physical and Engineering Sciences*, vol. 454, no. 1971, pp. 903–995, 1998.

[18] J. Gilles, "Empirical wavelet transform," *IEEE Trans. Signal Processing*, vol. 61, no. 16, pp. 3999–4010, 2013.

[19] Dragomiretskiy and D. Zosso, "Variational mode decomposition," *IEEE Transactions on Signal Processing*, vol. 62, no. 3, pp. 531–544, 2014.

[20] S. Meignen and D.-H. Pham, "Retrieval of the modes of multicomponent signals from downsampled short-time Fourier transform," *IEEE Transactions on Signal Processing*, vol. 66, no. 23, pp. 6204–6215, 2018.

[21] L. Stanković, "A measure of some time–frequency distributions concentration," *Signal Processing*, vol. 81, no. 3, pp. 621–631, 2001.

[22] R. G. Baraniuk, P. Flandrin, A. J. Janssen, and O. J. Michel, "Measuring time-frequency information content using the Rényi entropies," *IEEE Transactions on Information theory*, vol. 47, no. 4, pp. 1391–1409, 2001.

[23] L. Li, H. Cai, H. Han, Q. Jiang, and H. Ji, "Adaptive short-time Fourier transform and synchrosqueezing transform for non-stationary signal separation," *Signal Processing*, vol. 166, p. 107231, 2020.

[24] L. Li, H. Cai, and Q. Jiang, "Adaptive synchrosqueezing transform with a time-varying parameter for non-stationary signal separation," *Applied and Computational Harmonic Analysis*, 2019.

[25] R. Carmona, W. Hwang, and B. Torresani, "Characterization of signals by the ridges of their wavelet transforms," *IEEE Transactions on Signal Processing*, vol. 45, no. 10, pp. 2586–2590, Oct 1997.

[26] M. A. Colominas, S. Meignen, and D.-H. Pham, "Fully adaptive ridge detection based on stft phase information," *IEEE Signal Processing Letters*, 2020.